I&EC research
Industrial & Engineering Chemistry Research

Materials and Interfaces

Preparation of porous carbons from petroleum pitch and polyaniline by thermal treatment for methane storage

Paula Navarro-Quirant, Carlos Cuadrado-Collados, Aroldo Romero-Anaya, Joaquin Silvestre-Albero, and Manuel Martínez-Escandell

Ind. Eng. Chem. Res., **Just Accepted Manuscript** • DOI: 10.1021/acs.iecr.9b06501 • Publication Date (Web): 04 Mar 2020

Preparation of porous carbons from petroleum pitch and polyaniline by thermal treatment for methane storage

Navarro Quirant, P.; Cuadrado- Collados, C.; Romero-Anaya A.J.; Silvestre Albero, J.; Martinez Escandell, M.*

Laboratorio de Materiales Avanzados, Departamento de Química Inorgánica-Instituto Universitario de Materiales. Universidad de Alicante. Apartado 99, E-3080. Alicante, Spain

Abstract

The methane storage capacity of two series of activated carbons, obtained from a graphitizable (petroleum pitch) and a non-graphitizable precursor (polyaniline), has been evaluated after different thermal treatments. Both samples have been pyrolyzed and subsequently activated with KOH to obtain a highly developed microporous structure. After the synthesis, samples have been heat-treated at different temperatures, between 1000ºC and 1500ºC, to introduce structural changes that could have an effect in two parameters defining the methane adsorption capacity: the porosity and the density. The physicochemical characterization of the samples has shown that the activation process destroys the pre-graphitic structure, with a development of microporosity. However, during the subsequent thermal treatment, the graphitic order can be partially recovered, especially with the graphitizable material, together with a decrease in the micropore volume and an enhancement of the density. The electrical conductivity of the activated carbon obtained from a graphitizable precursor improves much more with an increase in the temperature of the thermal treatment than that of the activated carbon

obtained from a non-graphitizable precursor. It is worth highlighting the high methane adsorption capacities achieved with some of these samples, reaching values as high as 180 V/V. These values are among the highest reported in the literature so far.

Key words: petroleum residue; thermal treatment; porosity; methane storage; electrical conductivity

* Corresponding author. Phone: 34-965903537; Fax: 34-965903454 ; E-mail address: manolo.m@ua.es (M.Martinez-Escandell)

1. Introduction

Natural gas is considered a sustainable alternative energy source in the current market to substitute carbon and petroleum due to the associated environmental benefits (e.g., lower emissions of greenhouse gases, higher combustion efficiency, etc) [1]. In this sense, this energy source can be used for different purposes and it is considered, among all alternatives, one of the most versatile.

Currently, the research in this field has focused on the development of systems and new technologies that use natural gas as a fuel for transportation [2,3,4]. Natural gas can be compressed to allow its storage in fuel tanks. However, this technology requires certain storage conditions. For instance, to store enough amount of natural gas to give sufficient autonomy to a vehicle requires storing it at very high pressures, < 20 MPa [5]. Under these conditions it can be stored up to 230 V/V [6]. This means that 230 units of volume under atmospheric conditions (25 ºC and 1 bar) can be stored in a recipient per unit volume. Under these conditions an energetic density of 9.7 MJ/L can be achieved. However, despite achieving storage at these pressures, the autonomy in vehicles does not exceed 200-250 Km [6]. This value can be increased to 23 MJ/L when the gas is liquefied. However, to liquefy methane a temperature of -162 ºC is required, this low value being an important drawback for transportation and storage [6].

A recent alternative to improve the storage of methane in transportation is the use of porous materials such as MOFs [7-10], zeolites or activated carbons [5,6]. MOFs have an extraordinary large pore volume, thus making these materials interesting to obtain gas storage values proximate to those defined by DOE. However, these materials have sometimes low stability when they are submitted to a conforming step [5]. To solve this problem, new materials have been tested with the aim to obtain high adsorption capacities in materials with high mechanical resistance [5,6,8]. Recent studies reported

the preparation of HKUST-1 MOF in form of monolith that reported absolute volumetric methane and excess volumetric adsorption values of 259 and 230 V/V at 68 bar, respectively [11,12]. This monolith shows a delivery capacity, using the real bulk density, of 172 $cm^3(STP)cm^{-3}$ at 68 bar which are among the highest reported for monolithic materials, although the preparation of these monoliths are only tested in small monoliths [13]. Activated carbons have been recognized as one of the most important materials for gas storage [5,13]. Adsorption in activated carbons has advantages with respect to other materials, as the storage in carbon materials can take place at lower pressures, from 20 MPa down to 3.5 or 4.0 MPa, without decreasing the autonomy of the vehicle. This pressure reduction is very important because the gas deposits can be produced using lighter materials, with lower resistance to pressure. In addition, another advantage when using lower pressures concerns the possibility to build-up deposits with adaptable forms to non-usable spaces of the vehicle, so that materials and space of the vehicle can be optimized.

The methane adsorption capacity on activated carbons depends on the porosity and, also, their density [5]. For that issue, activated carbons with optimized values of porosity and packing density (high packing densities) are necessary [5]. The preparation of metal carbon composites may help to increase adsorption and final density [14]. The final goal in the optimization of this process is to achieve the values defined by the Department of Energy of United States (DOE), i.e., a methane adsorption capacity of 263 V/V or 0.5 g/g [15].

The adsorption process is strongly affected by the porous structure characteristics of the activated carbons. To this end, the selection of the raw material, the design of the preparation process and control of the activation conditions are highly important. For this application, these conditions have to be optimized to developed activated carbons

with a widely developed microporosity, pore size width between 0.8-1.1 nm [16, 17], and also, with a high packing density, although very narrow micropores, < 0.5nm, are not desired to avoid adsorption of molecules larger than methane, which may remain adsorbed during cycling [17].

Previous studies have shown that the amount of methane stored in an adsorbent-filled tank under 4 MPa pressure was four times higher than that of an empty tank [18,19]. Methane adsorption (at 25 °C) on commercially available activated carbons with apparent surface area from 1150 to 3250 m^2/g has been investigated with very promising results [20]. In these studies the authors have reported uptakes of 6.51 mmol g^{-1} at 3.93 MPa, 3.79 mmol g^{-1} at 3.45 MPa and 11.5 mmol g^{-1} at 3.45 MPa, for some of their commercial activated carbons.

Others authors have studied methane adsorption on activated carbons prepared by KOH activation, using as precursor a commercial styrene divinylbenzene ion-exchange resin [21]. The materials prepared with apparent surface areas up to 3870 m^2 g^{-1} were used in the methane adsorption at 20 °C and up to 800 mmHg, the higher value of adsorption showed was 1.68 mmol g^{-1} (27 mg/g)

In this work, two materials have been selected, a graphitizable carbon, which comes from a mesophase pitch obtained from a petroleum residue and a non-graphitizable carbon, obtained from the pyrolysis of polyaniline. Two series of activated carbons have been prepared starting from these two precursors. The prepared materials have been pyrolysed, activated with KOH and, subsequently, heat-treated under inert atmosphere at temperatures ranging from 1000 to 1500 ºC. The two activated carbons series have been characterized to study their physical and chemical properties and, also, they have been evaluated in the methane adsorption.

2. Materials and methods

2.1. Materials.

Two activated carbons have been prepared from two different precursors, a graphitizable carbon (DO) and another non-graphitizable carbon (PA). The first material is a mesophase pitch obtained from petroleum residues and the second one has been obtained by the pyrolysis of polyaniline.

2.2 Preparation of activated carbons

The preparation of materials has been carried out in three steps: pyrolysis, activation and thermal treatment.

The pyrolysis process took place in a horizontal quartz tube furnace. For the pyrolysis process, a 100 mL/min nitrogen flow was used, heating rate of 5 ºC/min from room temperature to 500ºC, and a soaking time of 1 h. Pyrolysed samples nomenclature includes the name of the precursor followed by C and the pyrolysis temperature, i.e. PAC500. This stage is important as porous development much depend on pyrolysis conditions. These conditions were selected based on previous experience producing KOH activated carbons using petroleum cokes and polyaniline, which allow to produce a large porous development.[16,22]

KOH allows to produce activated carbon with large methane adsorption capacity [5,6]. KOH activation method was performed by physical mixing, in absence of water, between the activating agent and the pyrolysed sample. Thus, 30.0 g of the activating agent were directly mixed at room temperature with 10.0 g of the pyrolysed precursors. A KOH/carbon ratio of 3/1 was used. After that, the mixture was milled in a ball mill at 300 rpm for 30 minutes to achieve a homogeneous mixture. The obtained mixture was activated in a horizontal furnace. A 100 mL/min nitrogen flow was used, heating rate of

5 ºC/min from room temperature to 800 ºC, and soaking time of 1 h. The prepared samples were first washed with HCl 10 %wt, to neutralize the excess of KOH, and afterwards with distilled water until reaching a neutral pH.

Finally, a thermal treatment of the activated carbons at different temperatures has been carried out, using 200 mL/min Argon flow, a heating at 3 ºC/min up to 1000ºC, 1200ºC, 1350ºC or 1500 ºC, maintaining the final temperature during 1 h.

The nomenclature of the different activated carbons includes the precursor and the temperature of the thermal treatment performed after the activation process. For example: sample DO1500 is an activated carbon obtained from DO heat treated at 1500 ºC.

2.3. Characterization of activated carbons

2.3.1. Morphological analysis.

The morphology of activated carbons was studied using scanning electron microscopy in a JEOL JEM-2010.

2.3.2. Textural properties.

The textural characteristics of the activated carbons have been evaluated by N_2 adsorption at -196 ºC and CO_2 at 0 ºC [11, 23] in a volumetric Autosorb-6B apparatus from Quantachrome. Before the analysis, the samples were outgassed at 250 ºC for 4 h. The BET equation was applied to the N_2-adsorption data to estimate the apparent BET surface area (S_{BET}). The Dubinin–Radushkevich (DR) equation was applied to the N_2-adsorption data, to determine the total micropore volume (pores size < 2 nm), and to the CO_2-adsorption isotherms to determine narrow micropore volume (pores size < 0.7 nm) [24]. Mesoporosity (V_{meso}) has been calculated as the difference between total pore volume at a relative pressure of 0.95 and the total micropore volume.

2.3.3. Powder X-ray diffraction

X-ray powder diffraction (XRD) patterns were measured on a Bruker D8-Advance diffractometer with a mirror Göebel using Cu Kα1 radiation (λ = 0.154 nm) at 40 kV and 40 mA, in the range of 2θ from 3º to 90º and a step size of 0.3º.

2.3.4. X-ray photoelectron spectra.

The X-ray photoelectron spectra were obtained using a VG-Microtech Mutilab 3000 system equipped with an electron energy analyzer operating with 9 channeltrons at constant transmission energy (Ep = 50 eV). Scanning energy from 279.28 eV to 298.28 eV for C; from 525.28 eV to 545.28 eV for Oxygen; and from 392.28 eV to 410 eV for N has been carried out.

2.3.5. Densities measurement

Bulk density, $\rho_{(bed)}$.

Bulk density (b; bulk or tap) is a key parameter when working with packed beds and can be defined as the weight of porous solid per volume. This volume includes the volume of pores, both opened and closed, and the space volume between the solid particles. An experimental procedure similar to that described by the D2854-89 ASTM method has been applied.

He density, $\rho_{(He)}$.

He densities have been obtained in a He-Pycnometer provided by micromeritics AccuPyc 1330.

Hg density, $\rho_{(Hg)}$.

Mercury density has been obtained using a POREMASTER-60GT from Quantachrome Instruments at a pressure of 2.8 MPa, assuming that at that pressure the interparticle space has been filled (0.2 μm pores).

Packing density, $\rho_{(packing)}$.

Density measurements applying pressure have been carried to reduce the interstitial space between particles. Therefore, materials with densities higher than bed densities can be obtained. For these measurements, an Instron 4411 Universal testing machine has been employed to determine the applied load and changes in dimensions with accuracy.

The applied procedure has been developed in our laboratory. For that purpose, two parallel plates have been used to compact the samples in mold. For the measurements, a FTIR cylindrical mold, 13 mm diameter, has been used. The height of the mold without sample is considered as the starting point. The height of the mold with the sample allows calculating the initial packing volume of the sample. Packing tests were carried out applying a load from 0 to 5 kN using a packing rate of 0.2 mm/min. Variations of the height of the mold allows to calculate the changes in packing volume with load. Also, packing density has been determined by pressing the activated carbon at a load of 10 kN using an uniaxial press.

2.3.8. Conductivity measurements.

The electrical conductivity of the prepared materials was calculated from resistance measurements obtained from the powder. Measurements were carried out in a home-made four-points probe equipment consisting in a cylindrical Teflon sample holder connected to a Kethley 2700 multimeter using copper electrodes. All the measurements

were carried using 100 mg samples and the same packing pressure.

2.3.9. Methane adsorption measurements.

CH_4 adsorption capacity at room temperature up to 40 bar was measured for all samples. Before any adsorption experiment the activated carbons were outgassed at 250 °C for 4 h. These measurements were carried out in homemade fully automated high-pressure manometric equipment (designed and constructed by the Advanced Materials Group (LMA), now commercialized as iSorbHP by Quantachrome Instruments.

3. Results and discussion.

3.1. Yields and textural characterization

The yields obtained after carbonization (61 % for DO and 43% for PA) and activation processes (63 % for DO and 46% for PA), are quite different when using the petroleum residue, DO, or polymeric precursor, PA. These divergences can be due to the different nature and chemical properties of the materials, a graphitizable carbon (DO) and a polymeric non-graphitizable carbon (PA). Table 1 shows that the yields obtained after the thermal treatment applied to the activated carbons are similar, around 89 % for DO-series and between 85 - 89 % for PA-series.

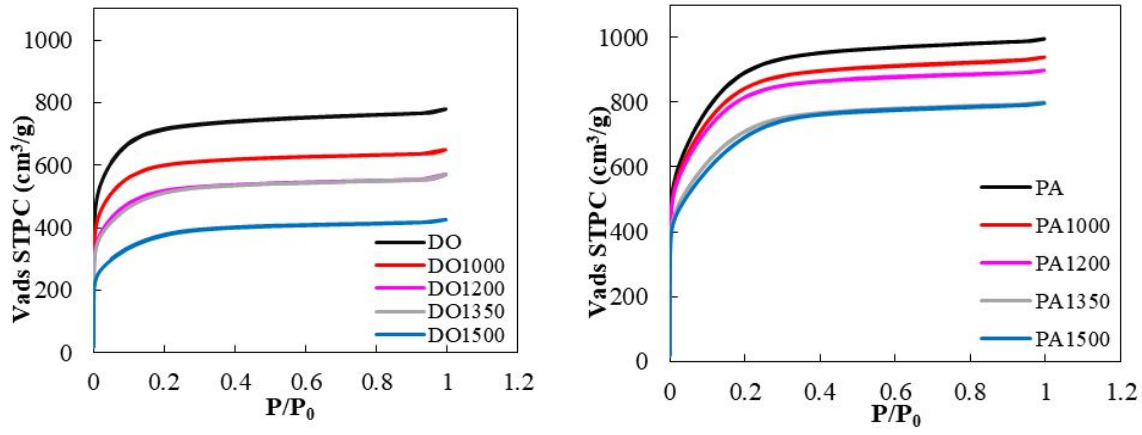

a) b)

Figure 1. N_2 adsorption isotherms at -196ºC of the prepared materials. (a) DO-series and (b) PA-series

Figure 1 shows the N_2 adsorption/desorption isotherms for the different samples prepared and Table 1 reports the yields obtained after thermal treatment. N_2 adsorption isotherms shown in Figure 1 are Type I, (according to IUPAC classification), characteristic of microporous materials. From this Figure it can be observed that the original activated carbons DO and PA exhibit the highest N_2 adsorption capacities while samples submitted to a thermal treatment exhibit a gradual decrease with temperature, especially for DO series. Figure 1 also shows that the pore size widens with an increase in the temperature of the thermal treatment, this widening being reflected in the knee of the nitrogen adsorption isotherm. The textural properties calculated from N_2 adsorption isotherms at -196ºC and CO_2 isotherms at 0ºC of the activated and heat-treated activated carbons are summarized in Table 1.

Table 1. Yields of thermal treatment, densities and textural properties of activated carbons prepared.

	Yield	Densities				Textural properties						
Sample	%	$\rho_{(He)}$	$\rho_{(bed)}$	$\rho_{(Hg)}$	$\rho^*_{(Packing)}$	S_{BET}	$V_{DR,N2}$	$V_{DR,CO2}$	$\mathbf{V_{meso}}$	$\mathbf{V_{total}}$	$V_{DR,N2}$	V_{meso}

		g/cm^3	g/cm^3	g/cm^3	g/cm^3	m^2/g	cm^3/g	cm^3/g	cm^3/g	cm^3/g	%	%
DOC500	-	-	-	--	-	-	-	-	-	-	-	-
DO	63	2.22	0.16	0.69	0.71	2650	1.04	0.51	0.16	1.21	86	14
DO1000	89	-	0.20	--	0.77	2200	0.87	0.43	0.14	1.01	86	14
DO1200	89	-	0.22	--	0.82	1860	0.76	0.38	0.12	0.88	86	14
DO1350	89	--	0.24	--	0.83	1800	0.72	0.41	0.22	0.89	81	19
DO1500	89	2.26	0.25	0.89	0.89	1300	0.51	0.28	0.15	0.66	87	13
PAC500	-	-	-		-	-	-	-	-	-	-	-
PA	46	2.11	0.15	--	0.53	3080	1.22	0.54	0.32	1.54	79	21
PA1000	84	-	0.17	0.60	0.52	2890	1.14	0.51	0.31	1.45	79	21
PA1200	87	-	0.18	--	0.65	2820	1.11	0.46	0.25	1.39	80	20
PA1350	88	-	0.19	--	0.63	2430	0.95	0.40	0.27	1.24	78	22
PA1500	89	2.26	0.17	--	0.64	2320	0.91	0.31	0.30	1.23	76	24

*Obtained at pressure of 76 MPa

Table 1 also includes the activated carbon yields after the heat-treatment. The apparent BET surface area, the micropore volumes ($V_{DR,N2}$) deduced from the Dubinin–Radushkevich equation and the mesopore volume were obtained from the nitrogen adsorption data, whereas the volume of narrow micropores ($V_{DR,CO2}$ < 0.7 nm) was calculated after applying the Dubinin–Radushkevich equation to the CO_2 adsorption data.

From Table 1, it is worth noting that PA activated carbon has the highest adsorption capacity with apparent surface area of 3080 m^2/g. This value gradually decreases till 2320 m^2/g when the treatment temperature has been increased up to 1500 ºC. DO activated carbon with an apparent surface area of 2650 m^2/g exhibits a decrease in the BET surface area down to 1300 m^2/g when the thermal treatment reaches 1500 ºC. It is worth noting that DO activated carbon has reduced almost 50% its surface area after a thermal treatment at 1500ºC, whereas carbons obtained from PA only decrease by 25%. These results are in good agreement with the behavior observed in the N_2 adsorption isotherms reported in Figure 1.

A similar tendency can be observed in the values of total microporosity and narrow microporosity. Larger values for total micropore volume ($V_{DR,N2}$= 1.34 cm^3/g)) and narrow micropore volume ($V_{DR,CO2}$= 0.51 cm^3/g) have been achieved for PA activated carbon, whereas samples heat-treated at 1500ºC exhibit a significant decrease. However, it is important to highlight that mesopore volumes do not change much and even increase after the heat treatments, especially with sample PA. It also has to be pointed out that the proportion of narrow microporosity with respect to the total microporosity is larger in the case of the DO series.

For a deeper analysis, the pore size distribution of the samples has been estimated from the N_2 adsorption data after application of the QSDFT method, Figures S1 a and b of supplementary material. In these Figures, it can be clearly observed the wider pore size distribution for the PA derived samples and the small changes occurring in the mesoporosity. However, the largest changes after the thermal treatment occur with microporosity, especially in DO series. In DO series the changes occur in pores lower than 1.6 nm, whereas in the PA samples the pores affected seems to be lower than 1.9 mn. In PA series, a decrease in all range of pores is observed, which seem to indicate that shrinkage of pores and coalescence of small pores is occurring. In the case of DO series, a similar behavior is observed, but in sample DO1500 the shrinkage of very small micropores is more evident and the smallest pores size has moved to higher values. The modification of porosity with heat treatment can be caused by pore shrinkage and coalescence of small pores, the former having a dominant role [25]. Emmerich [26] indicated that coalescence of crystallites along the c-axis occurs above 1000~1200°C for both graphitizable and nongraphitizable carbons, causing the superposition of different groups of graphite-like layers along the c-axis increase in L_c. Above this temperature changes are faster in the graphitizable material. It seems that in

the AC obtained from the graphitizable material, DO, the arrangements and layers alignments caused by the thermal treatment also have to be considered.

3.2. Densities.

Densities of the activated carbons, He density, bulk density and packing density, are summarized in Table 1. The results presented indicate that the temperature of the thermal-treatment has an important effect in the final density of the material due to the graphitic ordering rearrangement taken place. In the first place, He density of the starting activated carbons and the activated carbons heat-treated a 1500ºC are analyzed. For DO-series, density increases from 2.22 to 2.26 g/cm^3, indicative of the high density of the carbon skeleton of these carbons, which at 1500ºC reach the crystallographic density of graphite. In the case of the PA series, He-density increases from 2.11 to 2.26 g/cm^3 after the heat-treatment. In this case the starting density of the carbon skeleton is smaller as a result of the polymeric nature of the precursor, but increases to a similar value than that of DO carbon at the highest temperature of the heat treatment, i.e. 1500ºC.

A rather different behavior exhibit the values obtained for the bulk density. In this case, the density values for the PA-series increase with the temperature of the thermal treatment, from 0.15 to 0.19 g/cm^3, whereas the values obtained for DO-series present a larger increase, from 0.16 to 0.25 g/cm^3. This behavior is in good agreement with that observed when analyzing the changes in porosity, which seem to be larger for the DO series.

The measurement of packing density can give interesting information on how the carbon densifies when reducing the interparticle spaces. This density changes with the height of the carbon bed, i.e., with the pressure used to pack the carbon bed to reduce

the interparticle spaces. These measurements have been carried out using a Universal testing machine to measure load and volume changes with precision. Figure 2 shows the evolution of packing density with pressure for the two series of activated carbons. In general terms, all the activated carbons show a similar behavior: density increases fast below 2 MPa and increase linearly with pressure above 5 MPa. Almost all the series present a similar slope, the slope being larger for the DO series (0.0047-0.0051 g/cm^{3}MPa) than for the PA series (0.0038-0.0042 g/cm^{3}MPa), which may indicate a larger rigidity of the particles in the PA activated carbons.

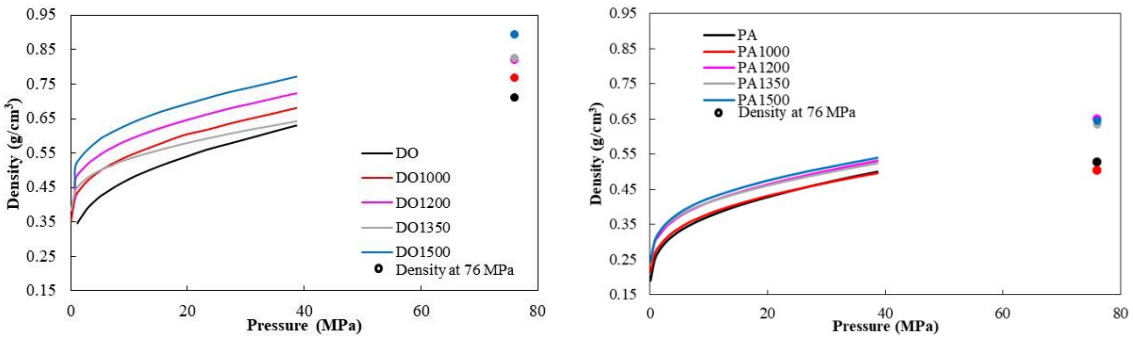

a) b)

Figure 2. Packing density of the prepared materials. (a) DO-series and (b) PA-series. Solid points indicate the density achieved at 76 MPa.

It also has to be pointed out that packing density for the activated carbons of DO series is larger than for those of PA series. The effect of temperature is also much more evident in DO series for which the increase of temperature results in a larger enhancement of the density. As the load cell of the Universal testing machine was only 5KN, an experiment with a larger pressure was carried out in a uniaxial press, using 76 MPa pressure. The results with the uniaxial press follow the same tendency. In fact, all densities for DO-series are above 0.65 g/cm^3, achieving a maximum value of 0.89 g/cm^3 for DO1500 sample. PA-series activated carbons have lower packing densities, their values being below 0.65 g/cm^3. This data indicate that the nature of the precursor is very

important, not only in the initial packing density but also in the way that they densify under pressure.

For the sake of comparison, mercury density of some of the samples has been measured, Table 1. These values have been obtained at a pressure higher than atmospheric, 2.8 MPa, to assure that Hg has penetrated in the interparticle space. Porosimetry curves of DO and DO1000 samples are included in supporting information, Figure S2. It is important to highlight the great similarities found in the values obtained using mercury porosimetry to those obtained at 76 MPa, Table 1. This agreement validates the measurement of packing density at 76 MPa. In any case, the values are always smaller that the values of He of density, which gives values of the carbon skeleton.

3.3. X-ray diffraction.

The effect of the temperature of the thermal treatment in the crystallinity of the activated carbons has been studied by X-ray diffraction. Figure 3 shows X-ray diffractograms for precursors PAC500, DOC500, and DO-series activated carbons (Figure 3a) and PA-series activated carbons (Figure 3b).

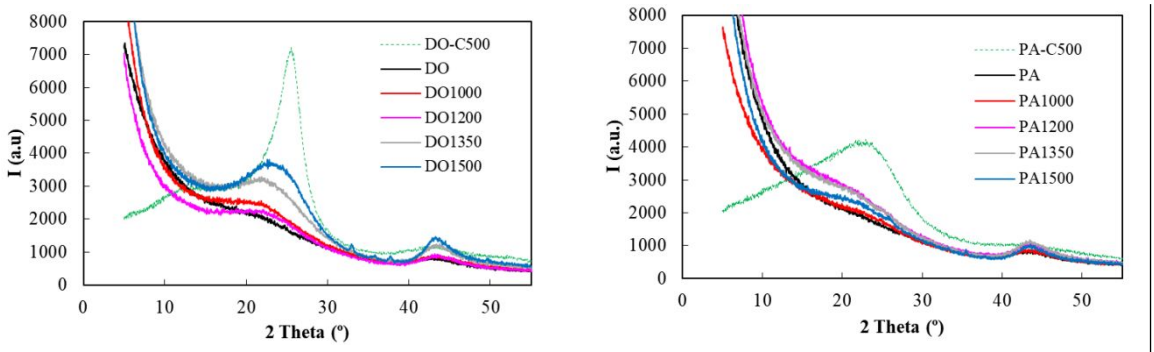

a) b)

Figure 3. DRX of all samples prepared. DO-serie (a) and PA-serie (b).

As it can be observed in Figure 3, the pyrolysed precursors, PA-C500 and DO-C500

samples, exhibit a characteristic peak of pregraphitic domains at 2θ ≈ 25º attributed to the (002) plane and two smaller, not very well-defined, contributions at 42-45º, attributed to (100), (101) planes of the graphite structure [27]. The first peak is more defined for the coke sample, DOC500, prepared from the graphitizable precursor, indicative of a large size of the packing of pregraphitic domains. In the case of the PAC500 this peak is wider, indicating a smaller size of the graphitic domains.

After KOH-activation, the carbon structure has been destroyed and, therefore, there is no presence of the graphite peaks in the difractograms of the activated carbons, DO and PA, Figure 2a,b. The drastic effect of the KOH activation treatment in the crystallinity of the activated carbons has been recently described in the literature, thus suggesting a random reorientation of the graphite microdomains after this harsh activation treatment [27].

Although DO sample has lost all the crystalline structure after activation, when this activated carbon is heat treated up to 1500ºC, samples DO1200, DO 1350 and DO1500, Figure 3 a, a gradual increase in the intensity of the (002) peak is easily appreciated indicating that the activated carbon is recovering part of its crystalline structure. This tendency has also been observed in the secondary peak at 2θ ≈ 45º corresponding for (001) plane. These results clearly show that although the graphitic structure was completely destroyed after the activation treatment with KOH, the graphitic microdomains can be easily reorganized after a high temperature thermal treatment.

However, Figure 3b shows that the effect of thermal treatment is not so relevant in PA activated carbons. Recovering graphitic structure seems to be much more difficult and only PA1500 sample shows a wide band on the (002) plane position. Thus, in the case of the non-graphitizable carbon, PA sample, the thermal treatment has a milder effect on the internal structure (non-appreciable reorganization), thus explaining the smaller

changes in textural properties due to the smaller pre-graphitic microdomains existing in the precursor. On the contrary, DO activated carbon has a larger capacity to reorganize and form graphitic crystals upon a heat treatment due to the presence larger size pre-graphitic units. It seems that the activation treatment with KOH destroys the ordering of the microdomains due to the harsh conditions used, but their re-arrangement is easier in the graphitizable material due to the large size of these units.

To analyze more in detail these results Bragg law has been applied to calculate the spacing between the planes of the crystal. These values have to be taken with precaution due to the low ordering of the carbon, although they have been used to analyze the structure of low ordering precursor such as pitches and asphaltenes providing useful information [28]. The results obtained are summarized in Table 2.

Table 2. X-ray difractions parameters of the carbons

	X-ray diffraction	
Sample	2θ (°)	d_{002} (Å)
DOC500	25.4	3.5
DO	-	-
DO1000	21.2	4.2
DO1200	22.1	4.0
DO1350	22.7	3.9
DO1500	23.9	3.7
PAC500	23.4	3.8
PA	-	-
PA1000	22.1	4.0
PA1200	22.3	4.0
PA1350	23.0	3.9
PA1500	23.7	3.8

Comparing the values obtained with PA500 and DO500 precursor with those of pure

graphite, 3.354 Å, it can be said that DOC500 (d_{002}=3.5 Å) has an interlayer spacing more proximate to graphite than PAC500 (d_{002}=3.8 Å). These results are expected since the original DO sample is a graphitizable material with a more organized structure. An increase of the interlayer space with activation is observed for DO and PA activated carbons, this occurring due to K intercalation within the activation process. In addition, the thermal treatment decreases the interlayer space with increasing temperature. However, there are not significant differences in the interlayer space between DO and PA series, indicative that the differences observed with porosity and density are more related to the size of precursor carbon layers than interlayer space.

3.4. Transmission Electronic Microscopy (TEM)

TEM has been employed to analyze the structural organization of the activated carbons before and after the thermal treatments. The original activated carbons and the carbons treated at 1500ºC show the largest structural changes. Figure 4 (a,d) shows the images for the activated carbons DO and PA and the treated carbons at 1500 ºC, DO1500 and PA1500.

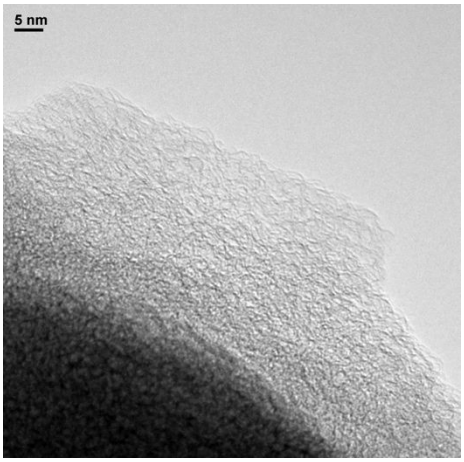

a)

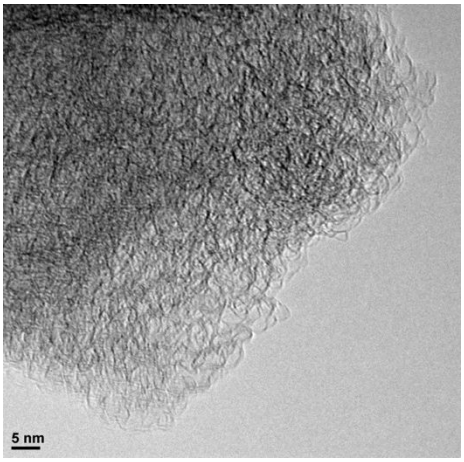

b)

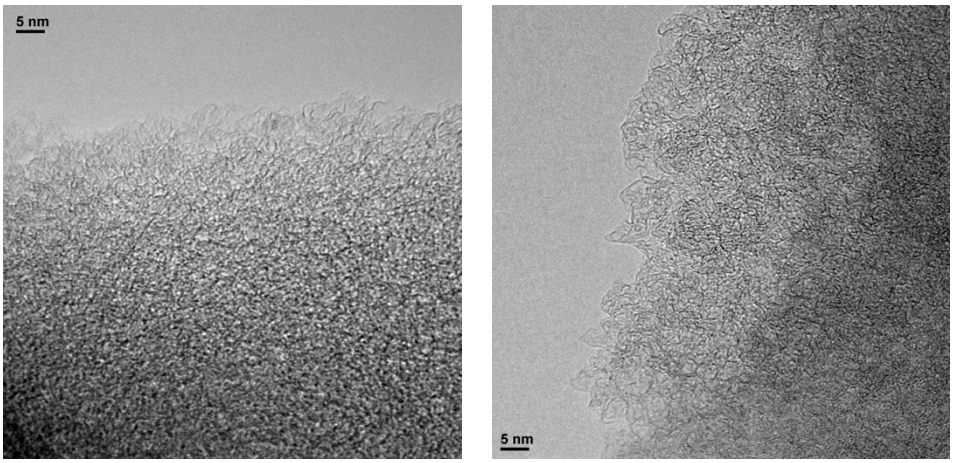

c) d)

Figure 4. TEM images of the samples DO (a), DO1500 (b), PA (c) and PA1500 (d).

Figure 4 (a and c) shows that the activated carbons DO and PA have a turbostratic structure, with very small crystal units, especially in sample PA. It seems that the activation process with KOH, as expected, destroys the crystalline structure of the initial material. However, after a thermal treated at 1500 ºC, it appears that the crystalline structure of the materials is reorganized again. Figure 4 (b and d) shows a re-organization of the crystalline structure of the materials after the thermal treatment, especially for sample DO1500, the enhancement of the crystalline units being clearly observed. This result confirms the results obtained by XRD.

3.5. X-ray photoelectron spectroscopy (XPS).

The adsorption properties of activated carbons depend on both the porous structure and the surface chemistry. The surface functional groups are usually bonded to the edges and corners of the aromatic sheets. The behavior of the carbon surface depends on the size and shape of sheets, the presence and location of the surface functionalities and π-electrons. XPS analysis allow to obtain information about the elemental composition of the outer layers of the activated carbon (with a depth of the analysis around 10-12 nm)

and the nature of these surface species. Figure 5 shows some representative XPS spectra obtained for PA series.

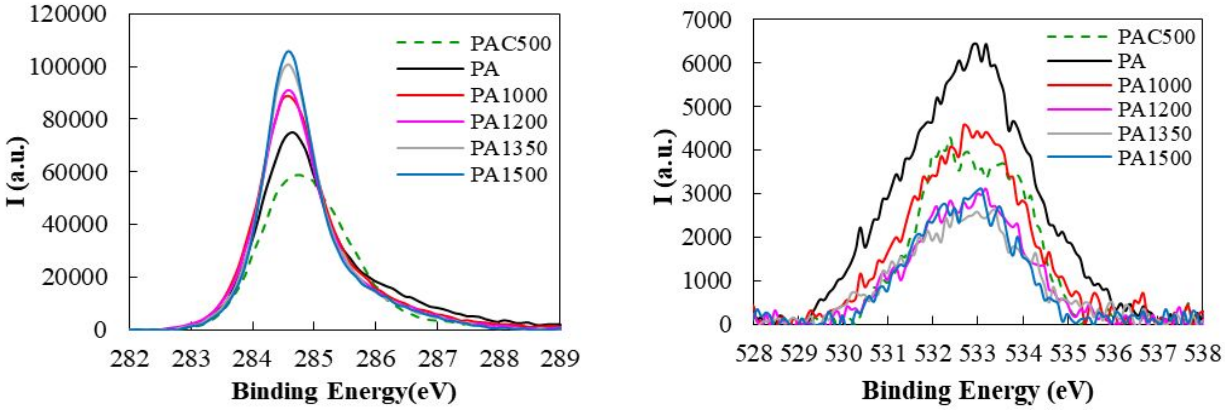

a) b)

Figure 5. XPS-spectra of PA-serie activated carbons. C1s peaks (a) and O1s peaks (b)

From Figure 5 it can be observed that, in general, for all samples evaluated the spectra consist of a single peak for C1s at around 284 - 285 eV, and a single peak for O1s at around 532 and 534 eV.

C1s and O1s contributions have been used for quantitative analysis of the elemental surface composition of the samples and to identify the chemical states of both elements.

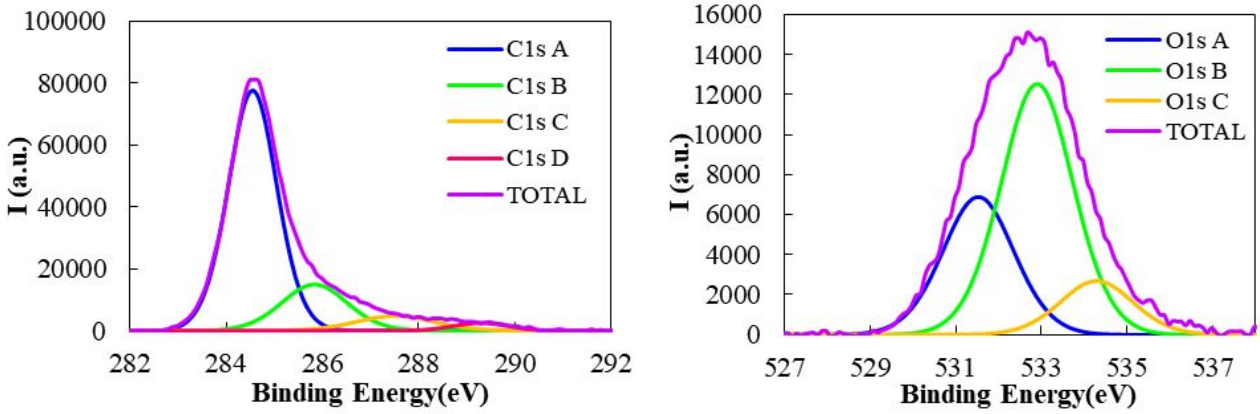

Figure 6. XPS-spectra of DO sample. Deconvolution of C_{1s} peak (a) and O_{1s} peak (b)

Figure 6 shows, as an example, the C_{1s} and O_{1s} spectrum for DO sample in which the signals for C1s and O1s have been deconvoluted.

The deconvolution of the C_{1s} spectrum could be considered in the forms of graphitized carbon, sp^2, at 284.6 eV, phenol, alcohol and ether around 286.2 eV, carbonyl around 288 eV, carboxylic or ester groups around 288.7 eV, and π–π* transitions around 290.5 eV. [29, 30].

The O_{1s} spectrum of sample also has also been deconvoluted into three components, corresponding to C=O groups (carbonyl groups) around 531.2 eV, C–OH or C–O–C groups (hydroxyl or ether) around 532.4 eV, and O=C–O groups (anhydride, lactone, or carboxylic acids) around 533.4 eV [30].

The quantification of the percentages of C, O and N, by deconvolution, of the peaks at different binding energy and different treatment temperatures are summarized in Tables 3 and 4.

In general terms, it seems that carbon content increases with temperature of the heat-treatment, whereas the percentage of O and N decreases when the treatment temperature increases, as a result of the decomposition of the superficial groups on the materials occurring when the treatment temperature is increased. In fact, N in the surface has almost disappeared during activation and cannot be detected a 1200ºC or higher temperatures.

DOC500 and PAC500 carbonized samples have a considerable carbon content, around 94 and 89 %, respectively; these values decrease with the KOH activation process and, after of thermal treatment increase with temperature. The oxygen content for DOC500 and PAC500 increase with the KOH activation process, from values of 5 and 4 % to values up to 11 and 6 %, respectively, but decreases afterwards with the thermal treatment, being lower than 2 % at 1500ºC. Thus, KOH activation process produces a modification in the surface composition of the precursor materials, decreasing carbon content due to the increase of oxygen surface groups.

Table 3. XPS characterization of activated carbons from DO-series

	DOC500	DO	DO1000	DO1200	DO1350	DO1500
Energy (eV)	Atomic Percentage of C (%)					
284.6	83.74	62.99	62.97	72.69	83.33	79.34
285.8	5.88	16.44	14.38	15.94	9.71	16.60
287.5	3.81	6.33	9.44	4.56	4.08	1.81
289.2	1.03	2.30	3.65	0.65	-	-
Total C	94.46	88.06	90.44	93.84	97.12	97.75
	Atomic Percentage of O (%)					
531.5	0.37	3.63	1.24	0.65	0.30	1.02
532.9	2.46	6.67	5.71	3.39	1.71	1.23
534.3	1.99	1.46	2.15	1.10	0.09	-
Total O	4.82	11.76	9.10	5.14	2.10	2.25
	Atomic Percentage of N (%)					
400.1	0.21	0.18	0.23	-	-	-
O/C	0.05	0.13	0.10	0.05	0.02	0.02

Table 4. XPS characterization of activated carbons from PA-serie

	PAC500	PA	PA1000	PA1200	PA1350	PA1500
Energy (eV)	Atomic Percentage of C (%)					
284.6	61.65	67.34	80.12	78.85	81.82	78.10
286.0	21.46	20.29	11.75	15.93	13.13	17.39
287.7	4.78	4.83	2.87	2.21	2.16	2.36
289. 8	1.21	0.94	1.52	0.54	0.69	-
Total C	89.10	93.40	96.26	97.53	97.80	97.85
	Atomic Percentage of O (%)					
531.3	0.31	1.72	1.03	0.72	0.79	0.76
532.9	1.80	3.31	2.36	1.74	1.41	1.39
534.5	1.64	1.05	0.36	-	-	-
Total O	3.75	6.08	3.75	2.46	2.20	2.15
	Atomic Percentage of N (%)					
398.38	4.58	-	-	-	-	-
400.17	2.58	0.51	-	-	-	-
Total N	7.16	0.51	-	-	-	-
O/C	0.04	0.07	0.04	0.03	0.02	0.02

Analyzing the data more in detail, it can be observed than for both the DO and PA series, activated carbons with sp^2 hybridization have a significant increase in the atomic percentage. However the functional groups C=O and COO-R, decrease their surface presence with the increase of the of the thermal treatments temperature, disappearing completely the COO-R group at high temperatures. In the case of oxygen groups, the

tendency is decreased. Activation generates hydroxyl and ether groups to a larger extent and when the temperature increases all the surface groups of the samples decreases, although COO-H groups seem disappear faster and at 1500ºC they have been evolved completely.

To conclude this analysis, from Table 3 it can observed that the O/C ratio of the materials decreased for the two series, which suggested a decreased of oxygen-confirming the decrease of functional groups when the treatment temperature decrease.

3.6. Electrical conductivity measurements

Electrical conductivity of carbon materials depends on the structural arrangements and porosity of the carbon. In general, the conductivity decreases with the pore volume of the carbon. Thus, the effect of activation and thermal treatment on the electrical conductivity has been evaluated.

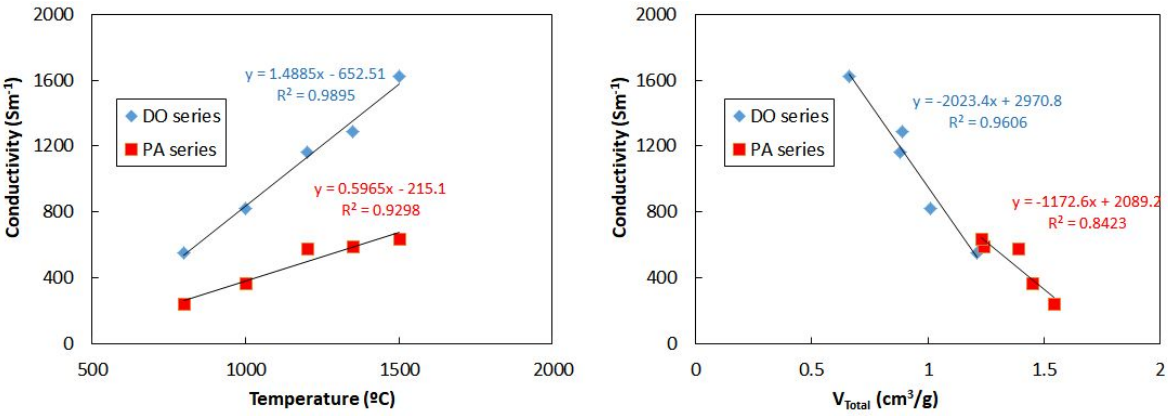

a) b)

Figure 7. Variation of electrical conductivity with: a) temperature of thermal treatment; b) total pore volume for DO and PA series of activated carbons.

Figure 7a shows the obtained conductivity values for the two series of activated carbons. For the sake of comparison, the electrical conductivity of two commercial activated carbons, RGC-30 and Maxsorb (MSC30), have been obtained using the same

procedure (values not included in the Figure), the obtained values being 210 Sm^{-1} and 640 Sm^{-1}, respectively. From Figure 7a it can be observed that the starting DO and PA activated carbons (without any thermal treatment) exhibit the lower conductivity values of the each series, 240 and 550 Sm^{-1}, respectively, these values being much lower for the carbon obtained from the polymeric precursor. In the case of PA, the value is similar to that measured for carbon RGC-30, whereas in the case of DO, the value is similar to Maxsorb MSC-30, a commercial KOH activated carbon. In both cases, conductivity increases significantly with the thermal treatment. A linear increase of conductivity with temperature is observed for both series, the slope being 3 times larger for the activated carbons obtained from the graphitizable precursor. In fact, only PA 1500 value is comparable to values obtain with pristine DO. At this point it is important to highlight that the conductivity values achieved with DO1500 are between 3 and 8 times larger than those of commercial activated carbon used.

Figure 7b present the evolution of electrical conductivity with total pore volume of the activated carbon, for the DO and PA series. For both series, a linear correlation with porosity is observed, DO series presenting the best adjustment. Electrical conductivity proportionally decreases with pore volume. It seems that the reduction of porosity, which contribution to the electrical conductivity is negligible, is the main responsible for the increase in conductivity observed. The larger slope for the graphitizable material, DO, and the larger value of conductivity at zero porosity indicates that the structural order of the carbon also affects. In this sense, the reduction of heteroatoms may also contribute to improve conductivity. These results are in good agreement with the results observed by textural characterization, XRD and TEM, indicating a faster recovery of the graphitizable structure in sample DO, with a considerable reduction of porosity, after a thermal treatment at high temperature.

Figures S3-S5 from supporting information present the relationship of electrical conductivity with other textural parameters. The adjustments observed do not improve those of porosity.

3.7. Methane adsorption

As a final application of this kind of materials, methane adsorption capacity has been evaluated. Figure 8 shows the methane adsorption isotherms for the two series of activated carbons prepared, DO and PA. Figure 8 a,b show the methane excess adsorption capacity expressed in gravimetric basis (volume of methane per grams of activated carbon - V/g) whereas Figure 8 c,d shows the methane excess adsorption capacity expressed in volumetric basis (volume of methane per volume of activated carbon - V/V). The latter values have been calculated using a packing density obtained at a pressure of 76 MPa. The values expressed as V/g are related to the textural properties of the carbon, especially microporosity [5, 6], whereas the values expressed as V/V are influence not only by porosity, but also by the density of the carbon.

In Figures 8 a,b can be observed that isotherms have a similar tendency; there is a continuous increase of the methane adsorption capacity when the pressure is increased, i.e. none of the samples reach saturation in the evaluated conditions. Sample DO and PA are similar below 30 bar, the differences between the samples are observed above that pressure. It seems that the higher proportion of pores larger than 1.5 nm of sample PA is the responsible for the higher capacity of this sample above 30 MPa. These differences in excess adsorption capacity should be greater if the adsorption takes place at pressure larger than 40 bars. Best adsorption values are obtained for the activated carbon DO and PA before any thermal treatment with values of 277 and 256 cm^3/g,

respectively (19.9 and 18.3 wt%).

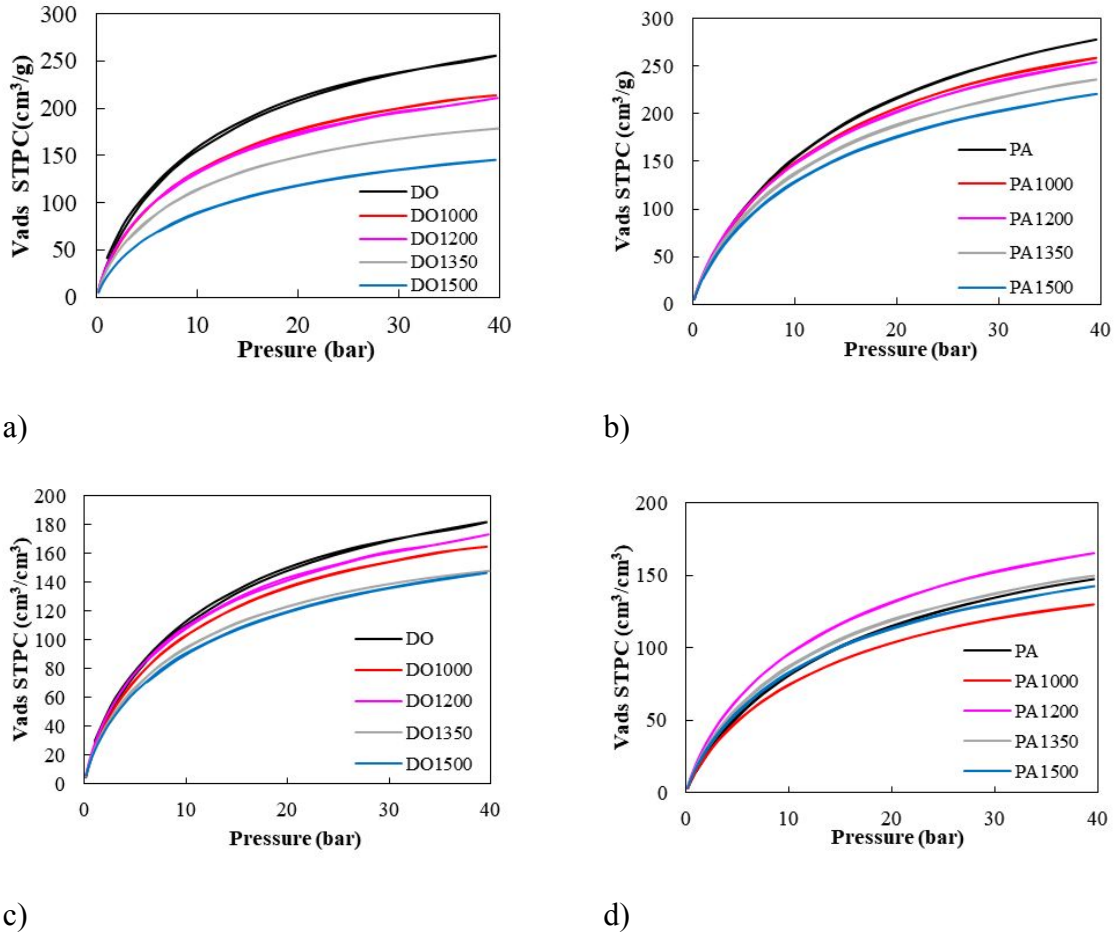

Figure 8. Methane adsorption isotherms. DO series (a and c), PA series (b and d)

At the same time, from Figure 8 a and b, it can be observed that, in both carbon series, the adsorption excess capacity decreases when the thermal treatment temperature increases, especially for DO series, with a more sensitive reduction (almost 2-fold decrease). This decrease mainly takes place at pressures below 20 bars, at a result of the observed decrease of microporosity with thermal treatment, which is mainly affecting pores below 1.5 nm.

The effect of thermal treatment not only affects to the textural properties but also to the degree of graphitization and the presence of heteroatoms. In this sense, the reduction of N and O surface groups and the increase of the graphitization degree of the carbon

contributes to improve the amount of methane adsorbed in the samples [31, 32]. However, it seems that the main effect that is influencing methane adsorption is the reduction of porosity.

Figure 8 c and d, shows the methane adsorption capacity when the packing densities of these materials (calculated using the packing density at 76 MPa) are employed to calculate the methane adsorbed capacity in a volumetric basis. From these Figures, it can be observed that the reduction of methane adsorption with the thermal treatment is much lower. In this case, the temperature produces a small decrease in the excess capacity, especially for DO series (Figure 8c), whereas for PA series there is not a clear tendency when the thermal treatment temperature increases (Figure 8d). Thus, methane adsorption decreases for PA1000 sample, but when the thermal treatment temperature is increased to 1200ºC (PA1200 sample) methane adsorption increases up to a value higher than the original PA sample. A further increase in the thermal treatment temperature, PA1350 sample, gives rise to a subsequent decrease in the methane adsorption capacity and, finally, the PA1500 sample has similar methane adsorption capacity than PA and PA1350 samples. From the values obtained, it has to be pointed out that when methane adsorption values are expressed as V/V, DO samples exhibit a better performance than PA samples, as a result of the larger packing density in the former carbons. The maximum adsorption capacity reached is 182 V/V for DO activated carbon, whereas for PA series the values cannot reach more than 160 V/V. Although it has not been possible to reach the DOE target under the applied experimental conditions, it is important to highlight that these values are among the best reported in the literature at 40 bar so far [33].

These values much depend on packing density of the carbon. This fact can clearly be observed in Figure 9 where the changes in methane adsorption (V/V) with packing

pressure can be observed. For this issue, the sample DO, which presented the highest volumetric adsorption for the packing density obtained a 76 MPa, has been selected. For the calculation, the gravimetric value at a methane pressure of 40 MPa has been chosen. It can be observed, that the methane adsorbed values increase fast with packing pressure and then increase linearly, as a result of the dependence of these values with packing density.

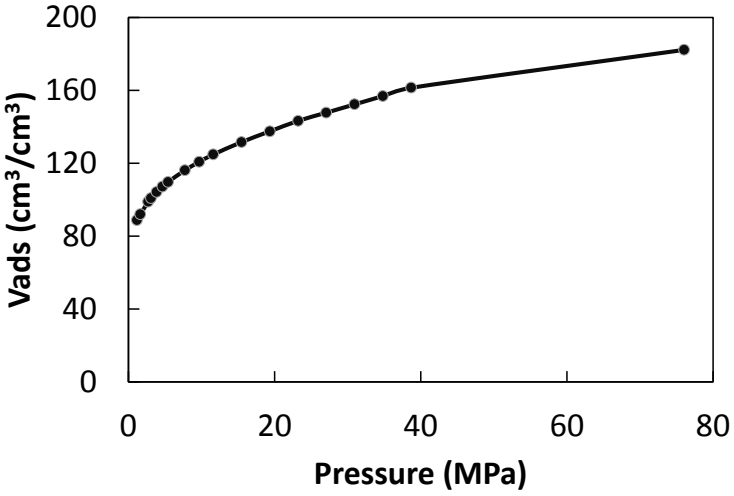

Figure 9. Methane adsorption (V/V) for DO activated carbon with packing pressure

Finally, an attempt has been made to correlate the methane adsorption values, expressed in V/g, with the textural parameters of the activated carbons. These measurements of methane adsorption do not depend on density of the material, but on the porous structure. The best correlation was found for the BET surface area and micropore volume.

The correlation of the adsorption values for the two series with the BET surface and micropore volume is presented, Figure 10, observing a similar fit for the two series. For other properties such as total pore volume, micropore volume and narrow micropore volume, correlations worsen and different correlations can be found depending on the

series of active carbon, see Figures S6-S9 of the Supplementary material.

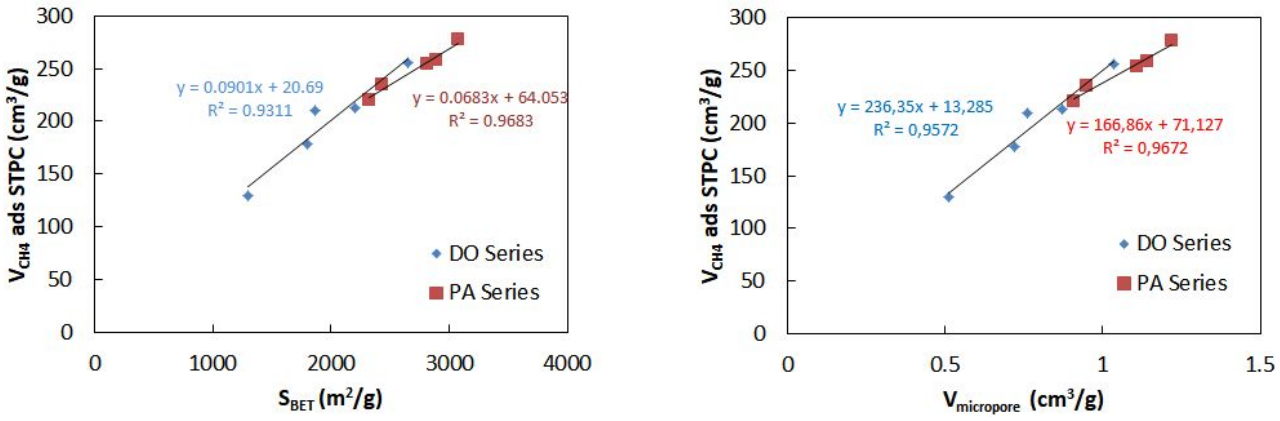

a) b)

Figure 10. Variation of the methane adsorption capacity with : a) apparent surface area, b) micropre volume, for DO and PA series.

4. Conclusions

Activated carbons were prepared from two precursors: a graphitizable carbon obtained from a petroleum residue, DO, and a non-graphitizable carbon obtained from the carbonization of polyaniline. The activated carbons were heat-treated up to 1500ºC. The activated carbons obtained were characterized and satisfactory employed to obtain methane adsorption measurements.

DRX and XPS analysis showed that KOH activation process destroys the initial pregraphitic structure of the two precursors. However, the carbon obtained using the most graphitizable carbon precursor, DO, recovers the graphitic structure to a larger extent with the thermal treatment. This fact affects to the porosity and packing density, so that the carbons obtained using DO densifies and decreases the porosity to a larger extent, whereas PA series changes in porosity and density are lower. In the same way, electrical conductivity improves with thermal treatment, increasing almost 4 times when the activated carbon DO is treated at 1500ºC. Additionally, it is remarkable that the electrical conductivity of the graphitizable precursor activated carbon, DO, improves

much more than that of the non-graphitizable precursor when increasing the temperature of heat treatment.

XPS analysis showed that the superficial groups were reduced considerably, especially the nitrogen groups with the thermal treatment.

The methane adsorption showed an increase when the apparent surface area increased. Also, the methane adsorption capacities for DO series have the higher methane adsorption capacities, achieving a maximum value of 180 V/V. This value is between the highest reported values recently.

Acknowledgments

Authors would like to acknowledge financial support from MINECO (MAT2016-80285-p)

5. References

[1] BP statistical review of world energy, BP, London, UK, 2019. https://www.bp.com/en/global/corporate/energy-economics/statistical-review-of-world-energy/natural-gas.html (accessed 28 July, 2019).

[2] Kowalczyk, P.; Tanaka, H.; Kaneko, K.; Terzyk, A.P.; Do, D.D. Grand canonical monte carlo simulation study of methane adsorption at an open graphite surface and in slit-like carbon pores at 273 K. *Langmuir.* **2005**, 21, 5639.

[3] Rodriguez-Reinoso, F.; Almansa, C.; Molina-Sabio, M. Contribution to the Evaluation of Density of Methane Adsorbed on Activated Carbon. *J. Phys. Chem. B*. **2005**, 109, 20227.

[4] Thallapally, P.K.; Kirby, K.A.; Atwood, J.L. Comparison of porous and nonporous materials for methane storage. *New J. Chem*. **2007**, 31, 628.

[5] Casco, M.E.; Martínez-Escandell, M.; Gadea-Ramos, E.; Kaneko, K.; Silvestre Albero, J.; Rodríguez-Reinoso, F. High-Pressure Methane Storage in Porous Materials: Are Carbon Materials in the Pole Position?. *Chem. Mater*. **2015**, 27, 959.

[6] Casco, M.E.; Martínez-Escandell, M.; Kaneko, K.; Silvestre-Albero, J.; Rodríguez Reinoso, F. Very High Methane Uptake on Activated Carbons Prepared from Mesophase Pitch: A Compromise between Microporosity and Bulk Density. *Carbon* **2015**, 93, 11.

[7] Vandenbrande, S.; Verstraelen, T.; Gutiérrez-Sevillano, J.J.; Waroquier, M.; Van Speybroeck, V. Methane Adsorption in Zr-Based MOFs: Comparison and Critical Evaluation of Force Fields. *J. Phys. Chem. C*. **2017**, 121, 25309.

[8] Dailly, A.; Beckner, M. Methane storage on metal-organic frameworks. Green energy and Technology. In *Nanoporous Materials for Gas Storage*; Kaneko, K., Rodríguez-Reinoso, F., Eds.; Springer: Singapore, 2019; pp 227-253.

[9] Eddaoudi, M.; Kim, J.; Rosi, N.; Vodak, D.; Wachter, J.; O'Keeffe, M.; Yaghi O.M. Systematic design of pore size and functionality in isoreticular MOFs and their application in methane storage. *Science*. **2002**, 295, 469.

[10] Zhao, D.; Yu, C.; Jiang, J.; Duan, X.; Zhang, L.; Jianag, K.; Qian, G. A fluorinated Zr-based MOF of high porosity for high CH_4 storage. *J. solid state chem*. **2019**, 277, 139.

[11] Mahmoud, E.; Ali, L.; Sayah, A.E.; Alkhatib, S.A.; Abdulsalam, H.; Juma, M.; Al-Muhtaseb, A.H. Implementing metal-organic frameworks for natural gas storage. *Crystals*. **2019**, 9, 1-19.

[12] Tian, T.; Zeng, Z.; Vulpe, D.; Casco, M.E.; Divitini, G.; Midgley P.A.; Silvestre-Albero, J.; Tan, J.; Moghadam, P.Z.; Fairen-Jimenez, D. A sol–gel monolithic metal–organic framework with enhanced methane uptake. *Nat. Mater*. **2018**, 17, 174.

[13] Marsh, H.; Rodríguez-Reinoso, F. *Activated Carbon*, 1st Edition, Elsevier Science: Amsterdam, **2006**.

[14] Djerndi, W.; Ben Mansour, N.; Ouederni, A.; Llewellyn, P.L.; El Mir, L. Elaboration of porous carbon/nickel nanocomposites for selective gas storage. *Solid state sci*. **2019**, 93, 37.

[15] Gallagher, J. Towards methane targets. *Nat Energy*, **2018**, 3, 86.

[16] Martinez-Escandell, M.; De Castro, M.M.; Molina-Sabio, M.; Rodriguez-Reinoso. F.; KOH Activation of Carbon Materials Obtained from the Pyrolysis of Ethylene Tar at Different Temperatures. *Fuel Process. Technol*. **2013**, 106, 402.

[17] Shen, J.; Dailly, A.; Beckner, M. Natural gas sorption on microporous materials. *Microporous Mesoporous Mater.* **2016**, 235, 170.

[18] Lozano-Castello, D.; Alcañiz-Monge, J.; de la Casa-Lillo, M.A; Cazorla-Amoros, D.; Linares-Solano, A. Advances in the study of methane storage in porous carbonaceous materials. *Fuel***, 2002**, 81, 1777.

[19] Morris, R.E.; Wheatley, P.S. Gas Storage in Nanoporous Materials. *Angew. Chem. Int. Ed.* **2008**, 47, 4966.

[20] Himeno, S.; Komatsu, T.; Fujita, S. High-Pressure Adsorption Equilibria of Methane and Carbon Dioxide on Several Activated Carbons. *J. Chem. Eng*. **2005**, 50, 369.

[21] Choma, J.; Osuchowski, Ł.; Dziura, A.; Marszewski, M.; Jaroniec, M. Benzene and Methane Adsorption on Ultrahigh Surface Area Carbons Prepared from Sulphonated Styrene Divinylbenzene Resin by KOH Activation. *Adsorpt. Sci. Technol*. **2015**, 33, 587.

[22] Silvestre-Albero A., Silvestre-Albero, J., Martínez-Escandell, M., Rodríguez-Reinoso, F. Micro/Mesoporous Activated Carbons Derived from Polyaniline: Promising

Candidates for CO_2 Adsorption. *Ind. Eng. Chem. Res.* **2014**, 53, 15398.

[23] Rouquerol, J.; Rouquerol, F.; Llewellyn, P.; Maurin, G.; Kenneth, S. Adsorption by Powders and Porous Solids: Principles, *Methodology and applications 2nd Edition*, Academic Press: New York, 2013.

[24] Lozano-Castelló, D.; Cazorla-Amorós, D.; Linares-Solano, A. Usefulness of CO_2 adsorption at 273 K for the characterization of porous carbons. *Carbon,* **2004**, 42, 1233.

[25] Kowalczyk, Z., Sentek, J., Jodzis, S., Diduszko, R., Presz, A., Terzyk, A.; Kucharski, Z; Suwalski, J. Thermally modified active carbon as a support for catalysts for NH_3 synthesis. *Carbon*, **1996**, 34, 403.

[26] Emmerich. F.G, Evolution with heat treatment of crystallinity in carbons. *Carbon*, **1995**, 33, 1709.

[27] Kun, P.; Wéber, F.; Balázs, C. Preparation and examination of multilayer graphene nanosheets by exfoliation of graphite in high efficient attritor mill. *Cent. Eur. J. Chem*. **2011**, 9, 47.

[28] Alvarez, A.G.; Martinez-Escandell, M.; Molina-Sabio, M.; Rodriguez-Reinoso, F. Pyrolysis of petroleum residues: analysis of semicokes by X-ray diffraction. *Carbon* **1999**, 37, 1627.

[29] Yang, G.X.; Jiang, H. Amino modification of biochar for enhanced adsorption of copper ions from synthetic wastewater. *Water Res*. **2014**, 48, 396.

[30] Swiatkowski, A.; Pakula, M.; Biniak, S.; Walczyk, M. Influence of the surface chemistry of modified activated carbon on its electrochemical behaviour in the presence of lead(II) ions. *Carbon*, **2004**, 42, 3057.

[31] Hao, S.; Wen, J.; Yu, X.; Chu, W. Effect of the surface oxygen groups on methane adsorption on coals. *Appl. Surf. Sci*., **2013**, 264, 433.

[32] Meng, J.; Li, S.; Niu, J.. Crystallite structure characteristics and its influence on

methane adsorption for different rank coals. *ACS Omega,* **2019**, 4, 20762

[33] Landers, J.; Gor, GY.; Neimark, AV. Density Functional Theory Methods for Characterization of Porous Materials. *Colloids Surfaces A Physicochem. Eng. Asp*. **2013**, 437, 3.

Figure Captions

Figure 5. N_2 adsorption isotherms at -196ºC of the prepared materials. (a) DO-series and (b) PA-series

Figure 2. Packing density of the prepared materials. (a) DO-series and (b) PA-series. Solid points indicate the density achieved at 76 MPa.

Figure 3. DRX of all samples prepared. DO-serie (a) and PA-serie (b).

Figure 4. TEM images of the samples DO (a), DO1500 (b), PA (c) and PA1500 (d).

Figure 5. XPS-spectra of PA-serie activated carbons. C1s peaks (a) and O1s peaks (b)

Figure 6. XPS-spectra of DO sample. Deconvolution of C1s peak (a) and O1s peak (b)

Figure 7. Variation of electrical conductivity with: a) temperature of thermal treatment; b) total pore volume for DO and PA series of activated carbons.

Figure 8. Methane adsorption isotherms. DO series (a and c), PA series (b and d)

Figure 9. Methane adsorption (V/V) for DO activated carbon with packing pressure

Figure 10. Variation of the methane adsorption capacity with : a) apparent surface area, b) micropre volume, for DO and PA series.

Supporting information

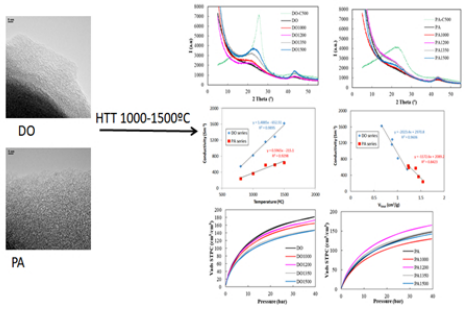

TOC graphic

254x190mm (96 x 96 DPI)